DALTON
FULL PAPER

Synthesis and structural characterization of mixed-metal Pt–Rh clusters. Assembly of tetra- and tetra-hexanuclear clusters from smaller metal fragments †

Igor O. Koshevoy,[a] Sergey P. Tunik,*[a] Sirpa Jääskeläinen,[b] Matti Haukka,[b] Tapani A. Pakkanen*[b] and Ivan S. Podkorytov[c]

[a] *Department of Chemistry, St. Petersburg State University, Universitetskii pr., 26, St. Petersburg, Staryi Peterhof 198504, Russian Federation. E-mail: stunik@st1323.spb.edu*
[b] *Department of Chemistry, University of Joensuu, P.O. Box 111, FIN-80101, Joensuu, Finland. E-mail: Tapani.Pakkanen@joensuu.fi*
[c] *S. V. Lebedev Central Synthetic Rubber Research Institute, Gapsalskaya 1, St. Petersburg, 198035, Russia*

Received 3rd January 2002, Accepted 17th April 2002
First published as an Advance Article on the web 21st May 2002

The tetranuclear cluster $[Rh_2Pt_2(CO)_6(dppm)_2]$ (**1**) has been obtained in good yield by redox condensation of $[Rh(CO)_4]^-$ with $[PtCl(dppm)]_2$ and also by substitution of two rhodium atoms in $[Rh_4(CO)_{12}]$ for the binuclear $[Pt_2(CO)_3(dppm)_2]$ fragment. The cluster **1** crystallizes in two isomeric forms, **1a** and **1b**, the former prevails both in solution and in the solid state. The molecular structures of both isomers have been established by X-ray analysis, which showed the presence of a tetranuclear butterfly framework with platinum atoms at the wingtip positions in the both clusters. The isomers differ from each other in the mode of dppm coordination on the cluster core. Reaction of the labile cluster $[Rh_6(CO)_{15}(NCMe)]$ with **1** results in formation of $[\{Rh_6(\mu_3\text{-}CO)_4(CO)_{10}\}(\mu_2\text{-}CO)_2\{Pt_2Rh_2(\mu_2\text{-}CO)_3(CO)_2(dppm)_2\}]$ (**2**), containing two cluster frameworks linked by a dative metal–metal bond. This cluster can also be obtained in slightly lower yield by reaction of $[PtCl(dppm)]_2$ with either $[Rh_7(CO)_{16}]^{3-}$ or $[Rh_6(CO)_{15}]^{2-}$. Treatment of $[Rh_6(CO)_{15}(NCMe)]$ with two equivalents of $[Pt_2(CO)_3(dppm)_2]$ affords $[\{Rh_6(\mu_3\text{-}CO)_4(CO)_{10}\}(\mu_2\text{-}CO)_2\{Pt_4(dppm)_3\}]$ (**3**), which displays another structural pattern containing the hexa- and tetranuclear cluster frameworks linked by a dative interaction. ^{31}P spectroscopic studies of **1a** and **2**, and simulation of the corresponding spectroscopic patterns showed that the structures of the "$Pt_2Rh_2(dppm)_2$" fragments found in the solid state remain unchanged in solution.

Introduction

The synthesis and chemistry of mixed-metal clusters attract considerable attention for various reasons, among which purely academic interest in the preparation of compounds with a desired cluster core composition[1,2] is accompanied by practical needs to obtain new and effective catalysts[3] and heterometallic phases with a known stoichiometry of the components.[4] In this respect, Pt–Rh compounds are of special interest due to the well-documented catalytic properties of the individual metals and their complexes in various organic reactions. In a previous publication,[5] we reported the synthesis of two mixed-metal tetra- and pentanuclear platinum–rhodium clusters. Further exploration of this chemistry resulted in the synthesis of a few novel compounds briefly described in a preliminary communication.[6] The present paper reports in detail the syntheses, structural characterization and spectroscopic studies of three platinum–rhodium clusters: $[Rh_2Pt_2(CO)_6(dppm)_2]$ (**1**), $[\{Rh_6(\mu_3\text{-}CO)_4(CO)_{10}\}(\mu_2\text{-}CO)_2\{Pt_2Rh_2(\mu_2\text{-}CO)_3(CO)_2(dppm)_2\}]$ (**2**), $[\{Rh_6(\mu_3\text{-}CO)_4(CO)_{10}\}(\mu_2\text{-}CO)_2\{Pt_4(dppm)_3\}]$ (**3**). The solid-state structures of the isomers of **1** have been established by X-ray crystallography, those of **2** and **3** were reported earlier.[6] Main features of the structures of **1**–**3** in solution have been verified by ^{31}P NMR studies and by simulation of the corresponding spectropic patterns.

† Electronic supplementary information (ESI) available: crystallographic data, atomic coordinates, bond lengths and angles, anisotropic displacement parameters, hydrogen coordinates and isotropic displacement parameters, and torsion angles for **1a** (Tables S1–S6) and **1b** (Tables S7–S12). See http://www.rsc.org/suppdata/dt/b2/b200003b/

Experimental

General comments

The starting complexes $[PtCl(dppm)]_2$,[7] $[Pt_2(CO)_3(dppm)_2]$,[8] $[Rh(CO)_4][PPN]$,[9] $[Rh_6(CO)_{15}][NBu_4]_2$,[10] $[Rh_7(CO)_{16}][NMe_4]_3$,[10] $[Rh_4(CO)_{12}]$,[11] $[Rh_6(CO)_{15}(NCMe)]$[12] were prepared according to literature procedures. All manipulations of the starting materials and products were carried out under atmospheres of nitrogen or carbon monoxide using standard Schlenk techniques. Reagent grade solvents—dichloromethane, hexane, acetonitrile, methanol, tetrahydrofuran, acetone and diethyl ether—were distilled over appropriate drying agents under an atmosphere of nitrogen prior to use. The solution ^1H, ^{31}P and 2D ^{31}P–^{31}P NMR spectra were recorded on a Bruker AM-500 spectrometer. The solid-state ^{31}P NMR experiment was run on a Bruker DSX 400 spectrometer. The chemical shifts were referenced to residual solvent resonances and external 85% H_3PO_4 in the ^1H and ^{31}P spectra, respectively. Fast atom bombardment (FAB+) mass spectra were obtained on a JEOL SX-102 instrument; 3-nitrobenzyl alcohol was used as a matrix and CsI as the calibrant. The observed isotopic distribution patterns fit completely to the calculated ones. IR spectra were

 DOI: 10.1039/b200003b

recorded on a Nicolet 550 Magna FTIR spectrometer. Microanalyses were carried out in the Analytical Laboratory of the University of Joensuu. The products were purified by column chromatography on silica, 5–40 mesh, Merck Kieselgel 60.

Syntheses

Synthesis of $[Rh_2Pt_2(CO)_6(dppm)_2]$ (1). *Method A.* $[Rh_4(CO)_{12}]$ (53 mg, 0.071 mmol) was dissolved in THF (7 cm^3) under a nitrogen atmosphere at room temperature. Crystalline $[Pt_2(CO)_3(dppm)_2]$ (180 mg, 0.145 mmol) was added to the solution, which darkened immediately. The reaction mixture was stirred for *ca.* 15 min. The solvent was then removed *in vacuo* to give an oily material, which was dissolved in 2 cm^3 of dichloromethane, diluted with 2 cm^3 of hexane (leaving some insoluble dark oily material) and transferred onto a chromatographic column (2.5 × 6 cm). Elution with CH_2Cl_2–hexane–Et_2O (2 : 5 : 0.2) gave one main orange band of $[Rh_2Pt_2(CO)_6(dppm)_2]$ (**1**) (89 mg, 41%). IR (CH_2Cl_2, cm^{-1}): ν(CO) 2027s, 2006s, 1810s br. ^{1}H NMR ($CDCl_3$): δ 7.93–6.18 (m br, Ph). $^{31}P\{^1H\}$ NMR ($CDCl_3$): δ −12.4 [2P, m, ^1J(P–Pt) 3258 Hz], 5.5 [2P, dm, ^1J(P–Rh) 168 Hz]. ^{31}P solid-state NMR: δ −20.9 [1P, ^1J(P–Pt) 2992 Hz], −14.5 [1P, ^1J(P–Pt) 3409 Hz], −10.0 [1P(Rh), br], 5.8 [1P(Rh), br]. FAB-MS (*m*/*z*): 1533 [M^-] (calcd 1532), [$M^+ - n$CO], n = 1–6. Anal. calcd for $C_{56}H_{44}O_6Rh_2Pt_2P_4$: C, 43.86; H, 2.87%. Found: C, 43.91; H, 2.89%.

Method B. $[PtCl(dppm)]_2$ (106 mg, 0.086 mmol) was suspended in anhydrous methanol (8 cm^3) and CO was bubbled through under vigorous stirring for 20 min. The resulting transparent solution was added dropwise, under a CO atmosphere, to crystalline $[Rh(CO)_4][PPN]$ (118 mg, 0.156 mmol). Immediate formation of a dark red solution and an orange crystalline precipitate was observed. The reaction mixture was diluted with degassed THF (2 cm^3) and stirred under CO for an extra 30 min. The solvents were removed *in vacuo* and the remaining solid was dissolved in 2 cm^3 of dichloromethane, diluted with 2 cm^3 of hexane (leaving some insoluble dark oily material) and transferred onto a chromatographic column (2.5 × 6 cm). Elution with CH_2Cl_2–hexane–Et_2O (2 : 5 : 0.2) gave one main orange band of $[Rh_2Pt_2(CO)_6(dppm)_2]$ (83 mg, 69%).

Single crystals of **1a** and **1b** suitable for X-ray studies were obtained by slow gas-phase diffusion of hexane into CH_3OH–THF solution under a nitrogen atmosphere.

Synthesis of $[\{Rh_6(\mu_3\text{-}CO)_4(CO)_{10}\}(\mu_2\text{-}CO)_2\{Pt_2Rh_2(\mu_2\text{-}CO)_3(CO)_2(dppm)_2\}]$ (2). *Method A.* $[PtCl(dppm)]_2$ (229 mg, 0.186 mmol) was suspended in dry methanol (12 cm^3) and CO was bubbled through under vigorous stirring for 20 min. The resulting transparent solution was added dropwise under a CO atmosphere to crystalline $[Rh_7(CO)_{16}][NMe_4]_3$ (170 mg, 0.122 mmol). Immediate formation of a dark red solution and a red–orange crystalline precipitate was observed. The reaction mixture was diluted with acetone (5 cm^3) and stirred under CO for an extra 30 min. The solvents were removed *in vacuo* and the remaining solid was separated using column chromatography [2.5 × 8 cm, eluant CH_2Cl_2–hexane–Et_2O (2 : 5 : 0.2)], to give two main bands in the order of elution: orange **1** (92 mg) and red $[\{Rh_6(\mu_3\text{-}CO)_4(CO)_{10}\}(\mu_2\text{-}CO)_2\{Pt_2Rh_2(\mu_2\text{-}CO)_3(CO)_2(dppm)_2\}]$ (**2**) (31 mg). The following spectroscopic characteristics were obtained for **2**: IR (CH_2Cl_2, cm^{-1}): ν(CO) 2088m, 2077w, 2054s, 2021mw, 1972vw, 1865w, 1787m br. ^{1}H NMR ($CDCl_3$): 7.87–6.51 (m br, Ph). $^{31}P\{^1H\}$ NMR ($CDCl_3$, 35 °C): −22.8 [m, 1P, ^1J(P–Pt) 2550 Hz], −16.5 [m, 1P, ^1J(P–Pt) 3190 Hz], −8.8 [dm, 1P, ^1J(P–Rh) 160, ^3J(P–P) 156 Hz], −7.45 [dm, 1P, ^1J(P–Pt) 3350, ^3J(P–P) 156 Hz]. Anal. calcd for $C_{71}H_{44}O_{21}Rh_8Pt_2P_4\cdot 0.5C_2H_5OH$: C, 33.32; H, 1.81%. Found: C, 33.73; H, 1.94%.

Method B. $[PtCl(dppm)]_2$ (82 mg, 0.067 mmol) was suspended in dry methanol (7 cm^3) and CO was bubbled through under vigorous stirring for 20 min. The resulting transparent solution was added dropwise to crystalline $[Rh_6(CO)_{15}][NBu_4]_2$ (100 mg, 0.066 mmol) under a CO atmosphere. Immediate formation of a dark red solution and a red–orange crystalline precipitate was observed. The reaction mixture was then diluted with degassed THF (4 cm^3) and stirred under CO for 30 min. The solvents were removed *in vacuo* and the remaining solid was dissolved in 2 cm^3 of dichloromethane, diluted with 2 cm^3 of hexane (leaving some insoluble dark oily material) and transferred onto a chromatographic column (2.5 × 8 cm). Elution with CH_2Cl_2–hexane–Et_2O (2 : 5 : 0.2) gave an orange band of **1** (19 mg) and a red band of **2** (42 mg).

Method C. $[Rh_6(CO)_{15}NCMe]$ (32 mg, 0.03 mmol) was dissolved in THF (10 cm^3), diluted with acetonitrile (2 cm^3) and added to crystalline $[Rh_2Pt_2(CO)_6(dppm)_2]$ (44 mg, 0.029 mmol) under nitrogen. The reaction mixture was stirred in the dark at room temperature under a nitrogen atmosphere for *ca.* 15 h. When a TLC spot test showed complete consumption of the starting compounds, the solvents were removed *in vacuo*. The remaining solid was dissolved in 2 cm^3 of dichloromethane, diluted with 2 cm^3 of hexane (leaving some insoluble dark material) and transferred onto a chromatographic column (2.5 × 7 cm). Elution with CH_2Cl_2–hexane–Et_2O (3 : 5 : 0.2) gave trace amounts of **1** and a main red band of **2** (49 mg, 66%).

Synthesis of $[\{Rh_6(\mu_3\text{-}CO)_4(CO)_{10}\}(\mu_2\text{-}CO)_2\{Pt_4(dppm)_3\}]$ (3). $[Rh_6(CO)_{15}NCMe]$ (36 mg, 0.033 mmol) was dissolved in THF (5 cm^3) under a nitrogen atmosphere. The solution was cooled down to *ca.* −50 °C and crystalline $[Pt_2(CO)_3(dppm)_2]$ (85 mg, 0.068 mmol) was added under vigorous stirring. The reaction mixture was slowly (*ca.* 1.5 h) warmed up to room temperature under a nitrogen atmosphere. The solvent was removed *in vacuo* from the reddish brown solution. The remaining solid was dissolved in 3 cm^3 of dichloromethane, diluted with 1.5 cm^3 of hexane (leaving some insoluble dark material) and transferred onto a chromatographic column (2.5 × 6 cm). Elution with CH_2Cl_2–hexane (2 : 1) gave trace amounts of **1** and a main red–brown band of $[\{Rh_6(\mu_3\text{-}CO)_4(CO)_{10}\}(\mu_2\text{-}CO)_2\{Pt_4(dppm)_3\}]$ (**3**) (62 mg, 63%). IR (CH_2Cl_2, cm^{-1}): ν(CO) 2083m, 2050s, 2020m, 1977m br, 1772m br. ^{1}H NMR (CD_2Cl_2): 7.16–6.76 (m br, Ph). $^{31}P\{^1H\}$ NMR (CD_2Cl_2, 20 °C): −4.8 [m, ^1J(P–Pt) 2970, ^2J(P–Pt) 450, ^3J(P–P) 195 Hz]. Anal. calcd for $C_{91}H_{66}O_{16}Rh_6Pt_4P_6$: C, 36.44; H, 2.20%. Found: C, 36.56; H, 2.45%.

X-Ray data collection and structure solution

The X-ray diffraction data were collected with a Nonius Kappa CCD diffractometer using Mo-Kα radiation (λ = 0.71073 Å). The Denzo and Scalepack[13] programs were used for cell refinements and data reduction. The structure of **1a** was solved by the Patterson method using the DIRDIF-99 program[14] and the WinGX graphical user interface.[15] Structure **1b** was solved by direct methods with the SIR97 program.[16] A multi-scan absorption correction based on equivalent reflections (XPREP in SHELXTL v. 5.1)[17] was applied to all data (T_{max}/T_{min} were 0.3937/0.2886 and 0.3850/0.2706 for **1a** and **1b**, respectively). Structural refinements were carried out with the SHELXL97 program.[18] The crystal structure of **1a** contained MeOH solvent. The solvent was partially lost from the crystals and it was refined with population parameter 0.5. The hydroxyl hydrogen of the MeOH molecule was located from the difference Fourier map and refined with constant U_{iso} = 0.06. All other hydrogens were placed in idealized positions and constrained to ride on their parent atoms. The crystallographic data are summarized in Table 1, and selected bond lengths and angles are listed in Table 2. The molecular structures of the complexes **1a** and **1b** are presented in Fig. 1.

Table 1 Crystallographic data for compounds **1a** and **1b**

	1a	**1b**
Empirical formula	$C_{56}H_{44}O_6P_4Pt_2Rh_2$	$C_{56.5}H_{46}O_{6.5}P_4Pt_2Rh_2$
Fw	1532.79	1548.81
Crystal system	Triclinic	Monoclinic
Space group	$P\bar{1}$	$P2_1/n$
a/Å	11.8198(4)	13.7311(2)
b/Å	12.5681(5)	29.1268(3)
c/Å	18.0603(7)	13.8315(3)
α/°	104.370(2)	90
β/	92.9790(10)	100.8680(10)
γ/°	95.5950(10)	90
V/Å^3	2578.49(17)	5432.59(15)
T/K	150(2)	120(2)
Z	2	4
D_{calc}/g cm^{-3}	1.974	1.894
μ/mm^{-1}	6.212	5.898
No. refl. collected	30924	31093
No. unique refl.	10456	8513
R_{int}	0.0341	0.0422
$R1$ [a]	0.0342	0.0288
$wR2$ [a]	0.0742	0.0643

[a] $I > 2\sigma$.

Table 2 Selected bond lengths and angles for **1a** and **1b**

1a		**1b**	
Bond lengths/Å			
Pt(1)–Rh(1)	2.7126(4)	Pt(1)–Rh(1)	2.6804(5)
Pt(1)–Rh(2)	2.7055(4)	Pt(1)–Rh(2)	2.6965(5)
Pt(1)–Pt(2)	2.9148(3)	Pt(1)–Pt(2)	3.0115(3)
Pt(2)–Rh(2)	2.6336(4)	Pt(2)–Rh(2)	2.6441(4)
Pt(2)–Rh(1)	2.6657(4)	Pt(2)–Rh(1)	2.6237(4)
Rh(1)–Rh(2)	2.7243(6)	Rh(1)–Rh(2)	2.6808(6)
Rh(1)–P(1)	2.2984(14)	Rh(1)–P(1)	2.3471(14)
Pt(2)–P(2)	2.2600(13)	Rh(2)–P(2)	2.3209(14)
Pt(2)–P(3)	2.2821(13)	Pt(2)–P(4)	2.2906(13)
Rh(2)–P(4)	2.2775(14)	Rh(1)–P(3)	2.2948(13)
Pt(1)–C(1)	1.880(7)	Pt(1)–C(1)	1.874(7)
Rh(1)–C(6)	1.899(6)	Pt(2)–C(4)	1.857(6)
Rh(2)–C(5)	1.914(6)	Rh(2)–C(6)	1.886(7)
Pt(1)–C(2)	2.081(6)	Pt(1)–C(2)	2.143(5)
Rh(1)–C(2)	2.091(6)	Rh(1)–C(2)	2.015(6)
Pt(1)–C(3)	2.096(6)	Pt(1)–C(3)	2.085(6)
Rh(2)–C(3)	2.052(6)	Rh(2)–C(3)	2.081(7)
Rh(2)–C(4)	2.094(5)	Rh(1)–C(5)	2.030(6)
Rh(1)–C(4)	2.102(5)	Rh(2)–C(5)	2.148(6)
C(1)–O(1)	1.121(8)	O(1)–C(1)	1.139(7)
C(2)–O(2)	1.145(7)	O(2)–C(2)	1.162(6)
C(3)–O(3)	1.157(7)	O(3)–C(3)	1.162(7)
C(4)–O(4)	1.153(6)	O(4)–C(4)	1.155(7)
C(5)–O(5)	1.143(7)	O(5)–C(5)	1.170(6)
C(6)–O(6)	1.142(7)	O(6)–C(6)	1.152(7)
Bond angles/°			
P(1)–Rh(1)–Rh(2)	137.18(4)		
P(1)–Rh(1)–Pt(2)	87.52(4)		
P(1)–Rh(1)–Rh(2)	137.18(4)		
P(2)–Pt(2)–Rh(2)	159.78(4)		
P(2)–Pt(2)–Rh(1)	97.99(4)		
P(2)–Pt(2)–P(3)	105.32(5)		
P(3)–Pt(2)–Rh(2)	94.90(4)		
P(3)–Pt(2)–Rh(1)	156.17(4)		
P(4)–Rh(2)–Rh(1)	134.92(4)		

CCDC reference numbers 176844 and 176845.

See http://www.rsc.org/suppdata/dt/b2/b200003b/ for crystallographic data in CIF or other electronic format.

Results and discussion

The tetranuclear cluster $[Rh_2Pt_2(CO)_6(dppm)_2]$ can be obtained in good yield *via* two different synthetic pathways:

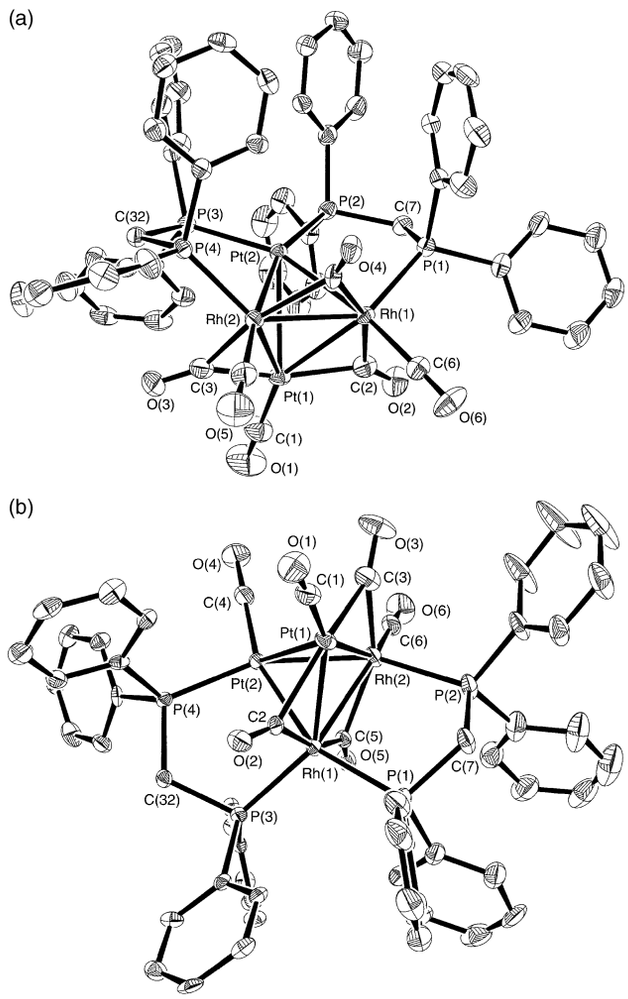

Fig. 1 Molecular structures of the $[Rh_2Pt_2(CO)_2(dppm)_2]$ isomers **1a** and **1b**. The thermal ellipsoids are drawn at the 50% probability level. Hydrogen atoms are omitted for clarity.

$$2[Rh(CO)_4][PPN] + [PtCl(dppm)]_2 \xrightarrow[\text{MeOH, 15 min}]{CO} [Rh_2Pt_2(CO)_6(dppm)_2] \quad \mathbf{1}, 69\% \qquad (1)$$

$$1/2[Rh_4(CO)_{12}] + [Pt_2(CO)_3(dppm)_2] \xrightarrow[\text{THF, 15 min}]{N_2} [Rh_2Pt_2(CO)_6(dppm)_2] \quad \mathbf{1}, 41\% \qquad (2)$$

The first reaction is an example of the well-established redox condensation of group 8 and 9 carbonylate anions with oxidized mono-, di- or triplatinum phosphine complexes,[19–24] whereas reaction (2) exemplifies a substitution of an Rh_2 for a Pt_2 fragment in the starting tetranuclear rhodium cluster. Despite the very different synthetic approaches used in reactions (1) and (2), the tetranuclear cluster **1** appeared to be the main product in both cases, which points to the particular stability of the Rh_2Pt_2 skeleton in the carbonyl–phosphine environment. The thermodynamic nature of this moiety is also corroborated by the emergence of **1** in reactions (3) and (4), see below, as a byproduct and by formation of the Rh_2Pt_2 framework as a part of the more complicated Rh_2Pt_2–Rh_6 structure in the same reactions. It is also worth noting that the analogous $[Rh_2Pt_2(CO)_7(PPh_3)_3]$ cluster was obtained previously as a major product in the reaction of $[Pt(PPh_3)_3]$ and $[Rh_4(CO)_{12}]$.[5]

Cluster **1** crystallizes in two isomeric forms, **1a** (major) and **1b** (minor), which only differ in the structure of their ligand

environments. The crystal and molecular structures of **1a** and **1b** in the solid state have been determined by X-ray diffraction analysis. ORTEP views of the both molecules are shown in Fig. 1, selected structural parameters are given in Table 2.

Both isomers are typical examples of 58 electron tetranuclear Pt_2M_2 clusters,[5,19,25] where four metal atoms form a tetrahedron with a substantially elongated Pt–Pt bond. This distance in **1a** and **1b** was determined to be 2.9148(3) and 3.0115(3) Å, respectively, which makes it possible to consider the frameworks as butterfly patterns. The other metal–metal distances in both clusters are significantly shorter and fall in the quite narrow ranges 2.634–2.724 and 2.624–2.697 Å, respectively. An essential structural feature of **1a** and **1b**, which has also been found in similar platinum-containing tetranuclear clusters,[5,19,26,25] consists of the Rh_2Pt triangle surrounded by three edge-bridging COs. The second platinum atom is bonded to this triangular face by two Pt–Rh bonds to form the structures shown in Fig. 1. In **1a**, the carbonyl bridges are essentially symmetrical, whereas in **1b**, C(2)O and C(5)O are shifted towards Rh(1), which bears two phosphorus atoms. Of the seven terminal sites available in these clusters, four are located at two rhodium atoms of the carbonyl-bridged triangle, one at Pt(1), which also belongs to the triangle, and the other two at Pt(2). These terminal sites are occupied by carbonyl and diphosphine ligands, the arrangement of which is quite different in the clusters of this type and evidently dictated by the stereochemistry of the phosphine ligands.

In the Pt_2M_2 clusters containing monophosphines,[5,19,25] these ligands occupy terminal positions at different metal atoms of the tetranuclear skeleton, probably reducing the interphosphine steric hindrances. In **1a**, **1b** and **2**, four phosphorus atoms of the diphosphine ligands are bonded to the metal triangle to form the structures (Fig. 1 and 3), where two terminal sites at one metal center are occupied by two phosphorus atoms. Formation of rigid five-membered Rh–P–C–P–Rh dimetallocycles reduces the steric hindrance of the phenyl substituents, which favours coordination of two phosphorus atoms to either platinum (**1a** and **2**) or rhodium (**1b**) centers. The metal to phosphorus and metal to terminal carbon bond lengths in **1a** and **1b** match well with the values found for other clusters of this sort.[5,19,25]

It is interesting that the ^{31}P NMR spectroscopic study of the bulk sample of **1** in the solid state as well as the NMR experiments in solution showed that the arrangement of the ligand sphere seen in **1a** is absolutely dominant and no spectroscopic evidence for the **1b** configuration was found. This evidently means that the relative amount of the latter isomer formed in synthetic experiments is below the sensitivity of ^{31}P NMR spectroscopy. However, it seems very likely that due to low solubility of **1b**, crystals of this complex have been seredipitously obtained and isolated in one of the crystallizations.

The solid-state ^{31}P NMR spectrum of **1** displays two multiplets typical of platinum-bonded phosphorus and two broadened resonances due to the rhodium-bonded phosphorus atoms, which is completely consistent with the slightly asymmetric solid-state structure of **1a** established by X-ray crystallography. The ^{31}P NMR spectrum of **1** recorded in solution, Fig. 2(A), showed that in the liquid phase, the connectivities of the phosphorus ligands with the cluster skeleton remain unchanged, in spite of the greater flexibility of the ligand sphere as a whole. The oscillation of the phosphorus atoms about the equlibrium positions results in the onset of a symmetry plane through the platinum atoms and the center of the Rh–Rh bond to reduce the number of signals in the spectrum to two multiplets, corresponding to platinum- and rhodium-bonded phosphorus nuclei, respectively. The high field signal displays a ^1J(Pt–P) of 3258 Hz, which fits well to the averaged values of the corresponding coupling constants observed in the solid-state spectrum. The solution ^{31}P spectrum can be simulated using a spin coupling model based on the

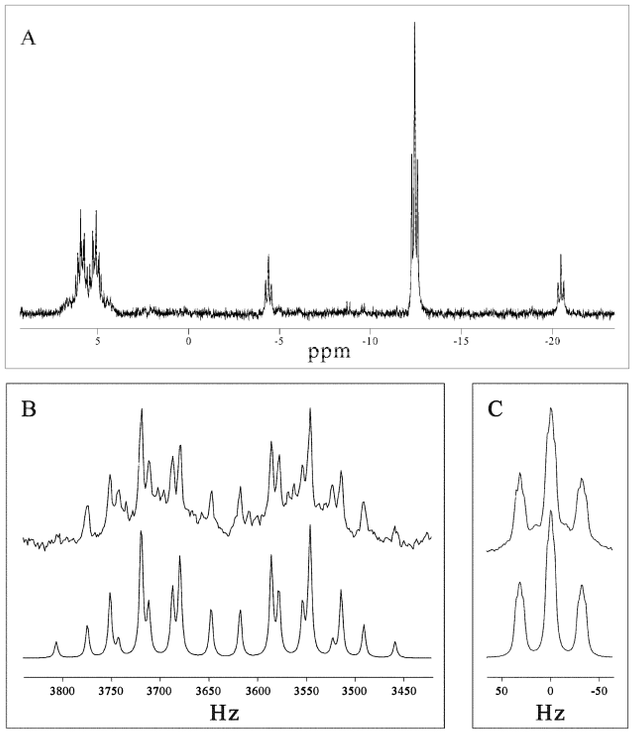

Fig. 2 202 MHz ^{31}P spectrum of $[Rh_2Pt_2(CO)_6(dppm)_2]$ (**1**) in $CDCl_3$ at T = 310 K. (A) Experimental spectrum. (B and C) Top trace: expansions of the experimental spectrum; bottom trace: simulations for the main isotopomer (containing no ^{195}Pt) spectrum. The (B) multiplet is *ca.* 2.5 times enlarged with respect to the (C) multiplet.

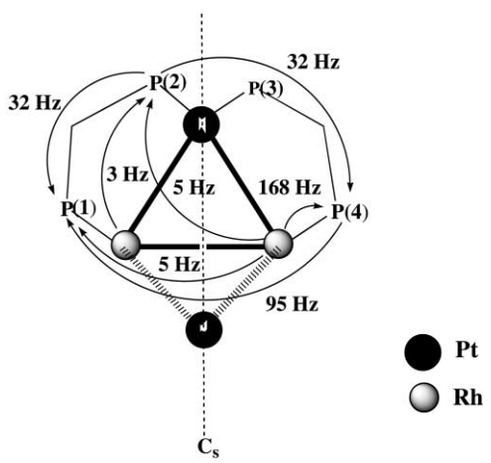

Chart 1

solid-state structure of **1a**, Chart 1. The one-bond phosphorus to platinum coupling constant has been measured directly from the experimental spectrum, whereas the other coupling parameters included in the model have been chosen to get the best fit to the experimental pattern. The two-bond coupling between the phosphorus atoms of dppm ligands [*e.g.* P(1)–CH_2–P(2)] has been introduced into the model with a value of 32 Hz, which is quite close to the previously reported data for dppm-containing $[Rh_6(CO)_{16}]$ derivatives (44.6[27] and 47.5 Hz[28]). The platinum-coordinated P(2) and P(3) nuclei are coupled with *trans* and *cis* rhodium atoms with ^2J(Rh–P) of 5 and 3 Hz, respectively. A similar two-bond Rh–P(1) coupling has also been put into the model. These magnitudes agree well with the analogous two-bond coupling constant (8 Hz) found in the $[Rh_6(CO)_{16}]$ triphenyl phosphite-substituted clusters.[28,29] Long range ^{31}P–^{31}P couplings in transition metal clusters are highly sensitive to the mutual disposition of the phosphorus atoms in the molecule under consideration. This results in the quite broad range of coupling constants observed in platinum

and rhodium clusters,[5,21–23,30,31] which lie in the interval from 16[23] to 256 Hz.[21] This sensitivity is especially indicative for the isomers of the $[Rh_6(CO)_{14}(P(OPh)_3)_2]$ cluster[30] containing *trans–trans* and *trans–cis* configurations of the phosphorus ligands, the corresponding coupling constants are 182 and 18.7 Hz, respectively. In line with this trend, we incorporated 32 and 95 Hz values as the ^3J(P–P) constants for the *trans–cis* P(1)–P(3) and P(2)–P(4), and *trans–trans* P(1)–P(4) couplings, respectively. Simulated patterns based on the above coupling model are given in Fig. 2(B, C).

The simulation has been done for the main isotopomer (no ^{195}Pt) only, but it can be easily seen that essential features of the experimental spectrum are adequately reproduced in both simulated patterns, except for the lack of long range ^{195}Pt satellites in the low field multiplet. A correct simulation of these satellites is hampered by their low intensity in the experimental pattern, which is comparable with the noise level. Nevertheless, the simulated patterns clearly support the coupling model suggested for **1a** and point to retention of the cluster solid-state structure in solution.

Two attempts to combine high nuclear rhodium carbonilate anions with the $[PtCl(dppm)]_2$ complex in the redox condensation reactions

$$[Rh_7(CO)_{16}]^{3-} + [PtCl(dppm)]_2 \xrightarrow[MeOH,\ 15\ min]{CO} \mathbf{1} + {}^{-} \quad (3)$$
59%

$$[\{Rh_6(\mu_3\text{-}CO)_4(CO)_{10}\}(\mu_2\text{-}CO)_2\{Pt_2Rh_2(\mu_2\text{-}CO)_3(CO)_2(dppm)_2\}]$$
2, 15%

$$[Rh_6(CO)_{15}]^{2-} + [PtCl(dppm)]_2 \xrightarrow[MeOH,\ 15\ min]{CO} \mathbf{1} + \mathbf{2} \quad (4)$$
56% 37%

resulted in formation of **1** along with a new polynuclear complex containing Rh_6 and Rh_2Pt_2 fragments linked by a Rh–Rh bond supported by two bridging CO ligands. The crystal and molecular structure of **2** has been established previously[6] by an X-ray crystallographic study. The molecular structure of **2** is shown in Fig. 3, selected bond lengths and angles are given in Table 3.

The cluster **2** can be obtained in higher yield by direct coupling of two neutral molecules,

$$[Rh_6(CO)_{15}(NCMe)] + [Rh_2Pt_2(CO)_6(dppm)_2] \xrightarrow[THF,\ 15\ min]{N_2} \mathbf{2} \quad (5)$$
66%

one of which is a typical "lightly stabilized" cluster widely used to insert a two electron donor into the coordination sphere of $[Rh_6(CO)_{16}]$.[12,29,32–34] In reaction (5), both the starting clusters contain "ready to be coupled" metal skeletons that gave a higher yield of the coupled product **2**. However, the rate of reaction (5) is slower as compared with rates of reaction (3) and (4) and much slower than the rate of acetonitrile substitution in $[Rh_6(CO)_{15}(NCMe)]$ for the phosphorus donors.[32] The slowness of reaction (5) may very likely arise from the difference in dppm coordination in **1a** and **2** that calls for rearrangement of the $[Rh_2Pt_2(dppm)_2]$ fragment to make possible coupling of these clusters.

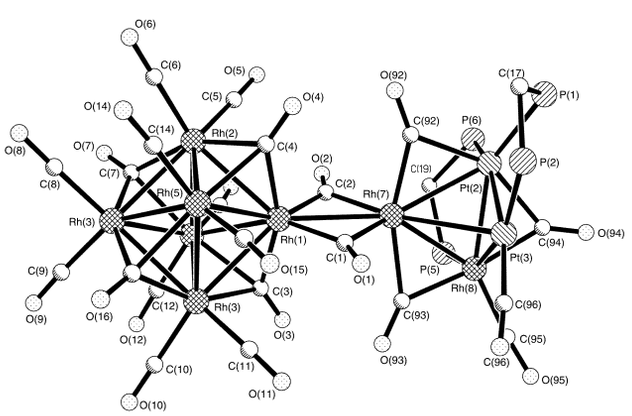

Fig. 3 Structure of $[\{Rh_6(\mu_3\text{-}CO)_4(CO)_{10}\}(\mu_2\text{-}CO)_2\{Pt_2Rh_2(\mu_2\text{-}CO)_3(CO)_2(dppm)_2\}]$ (**2**).[6]

Table 3 Selected bond lengths in **2** and **3**

Bond lengths in **2**/Å		Bond lengths in **3**/Å	
Rh(1)–Rh(2)	2.7841(5)	Rh(1)–Rh(2)	2.7782(4)
Rh(1)–Rh(4)	2.7985(4)	Rh(1)–Rh(4)	2.7738(4)
Rh(1)–Rh(5)	2.7822(5)	Rh(1)–Rh(5)	2.7878(4)
Rh(1)–Rh(6)	2.8047(5)	Rh(1)–Rh(6)	2.7739(4)
Rh(2)–Rh(3)	2.7489(5)	Rh(2)–Rh(3)	2.7469(4)
Rh(2)–Rh(5)	2.7925(5)	Rh(2)–Rh(5)	2.7170(5)
Rh(2)–Rh(6)	2.7118(5)	Rh(2)–Rh(6)	2.8151(5)
Rh(3)–Rh(4)	2.7524(5)	Rh(3)–Rh(6)	2.7491(5)
Rh(3)–Rh(5)	2.7480(5)	Rh(3)–Rh(4)	2.7536(5)
Rh(3)–Rh(6)	2.7521(5)	Rh(3)–Rh(5)	2.7632(5)
Rh(4)–Rh(5)	2.7150(5)	Rh(4)–Rh(5)	2.7846(5)
Rh(4)–Rh(6)	2.7901(5)	Rh(4)–Rh(6)	2.7236(5)
C(3)–Rh(1)	2.115(4)	Rh(1)–C(3)	2.044(4)
C(3)–Rh(6)	2.229(4)	Rh(4)–C(3)	2.311(4)
C(3)–Rh(4)	2.314(4)	Rh(5)–C(3)	2.318(4)
C(4)–Rh(1)	2.121(4)	Rh(1)–C(4)	2.168(4)
C(4)–Rh(5)	2.234(4)	Rh(2)–C(4)	2.224(4)
C(4)–Rh(2)	2.283(4)	Rh(6)–C(4)	2.240(4)
C(7)–Rh(2)	2.159(5)	Rh(3)–C(16)	2.222(5)
C(7)–Rh(6)	2.167(5)	Rh(4)–C(16)	2.144(4)
C(7)–Rh(3)	2.228(5)	Rh(6)–C(16)	2.162(4)
C(16)–Rh(5)	2.148(5)	Rh(2)–C(7)	2.165(4)
C(16)–Rh(4)	2.158(4)	Rh(3)–C(7)	2.202(5)
C(16)–Rh(3)	2.209(5)	Rh(5)–C(7)	2.147(4)
C(92)–Rh(7)	2.013(4)	Pt(2)–P(6)	2.2575(11)
C(92)–Pt(2)	2.225(4)	Pt(2)–P(1)	2.2782(10)
C(93)–Rh(8)	2.107(4)	Pt(3)–P(3)	2.2682(10)
C(93)–Rh(7)	2.130(4)	Pt(3)–P(2)	2.2932(10)
C(94)–Rh(8)	1.982(4)	Pt(4)–P(4)	2.2748(10)
C(94)–Pt(2)	2.178(4)	Pt(4)–P(5)	2.2791(11)
C(95)–Rh(8)	1.888(5)		
C(96)–Pt(3)	1.888(5)		
P(1)–Pt(2)	2.3214(11)		
P(2)–Pt(3)	2.2950(11)		
P(5)–Rh(8)	2.3441(11)		
P(6)–Pt(2)	2.3414(11)		

As shown in our preliminary communication,[6] the bonding between two cluster units in **2** can be rationalized on the basis of a dative bond between hexa- and tetranuclear metal fragments. The structure of the "$Rh_6(CO)_{14}$" fragment in **2** then represents a standard example of the non-ionic $[Rh_6(CO)_{16}]$-substituted derivatives[30,35,36] The substitution of a terminal CO in $[Rh_6(CO)_{16}]$ for a stronger donor ligand results in some typical structural distortions observed in the vicinity of the substitution site.[33] In particular, two adjacent face-bridging COs are substantially shifted to the substituted metal atom from idealized position over the centre of the rhodium triangle. The same trend is observed in **2**, where C(3)O and C(4)O ligands, adjacent to the Rh(1) atom bonded to the Rh_2Pt_2 donor fragment, are shifted to this metal atom, the difference between the shortest and longest carbon to rhodium bond being 0.2 Å, whereas the remote C(3)O and C(4)O groups are coordinated in an essentially symmetric manner. These observations indirectly point to similarity of the $\{Rh_2Pt_2\} \longrightarrow \{Rh_6\}$ dative bonding mode to that between a regular two electron donor ligand and the Rh_6 cluster core.

The bonding between the Rh_2Pt_2 and Rh_6 fragments in **2** very likely forces rearrangement of the diphosphines coordination as compared with the "parent" cluster **1a**. This rearrangement minimizes van der Waals interaction between the bulky Rh_6 moiety and the dppm ligands of the Rh_2Pt_2 fragment. The Rh(1)–Rh(7) bond length, 2.7684(5) Å, is comparatively

shorter than the analogous distance in the $[Rh_{12}(CO)_{30}]^{2-}$ dianion, 2.812 Å.[37] The Rh_2Pt_2 framework adopts a butterfly configuration with Rh(7) and Pt(3) atoms at wingtip positions, the Rh(7)–Pt(3) distance is 2.9575(4) Å. This distinguishes **2** from **1a**, **1b** and other butterfly M_2Pt_2 clusters,[5,36,38] where two platinum atoms are normally found at the wingtip sites of the butterfly framework. It is also of note that the Rh_2Pt_2 framework is surprizingly stable, remaining intact in reaction (5), which results in the change of its electron configuration from 58 to 56 electrons.

The ^{31}P NMR spectrum of **2** displays three platinum multiplets centered at −22.8, −16.5 and −7.45 ppm, $^1J(Pt–P)$ = 2550, 3190 and 3350 Hz, respectively, and a doublet due to the P(2) phosphorus atom bonded to Rh(8), −8.8 ppm, $^1J(Rh–P)$ = 160 Hz, that fits completely with the structure found in the solid state. This spectroscopic pattern can be simulated in the way shown in Fig. 4, taking into account additional long range

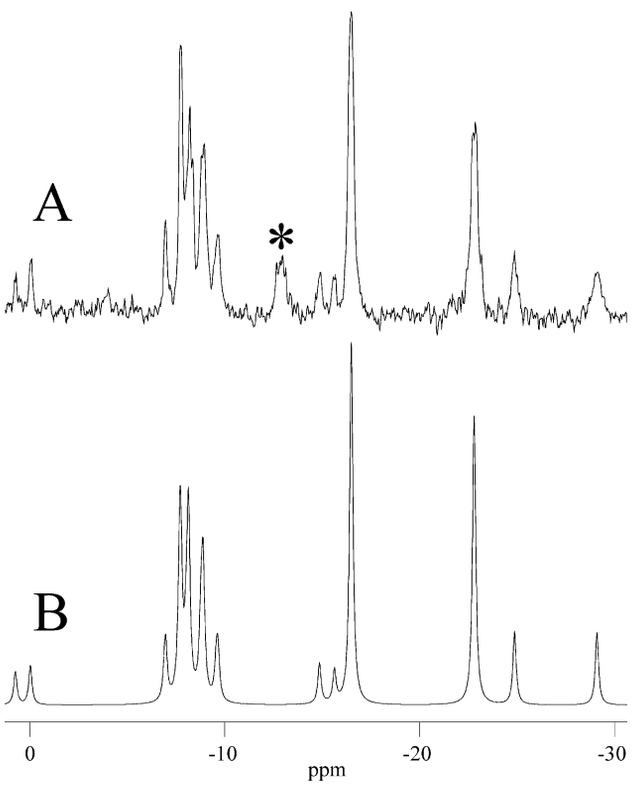

Fig. 4 202 MHz $\{^1H\}^{31}P$ spectra of $[\{Rh_6(\mu_3\text{-}CO)_4(CO)_{10}\}(\mu_2\text{-}CO)_2\{Pt_2Rh_2(\mu_2\text{-}CO)_3(CO)_2(dppm)_2\}]$ (**2**) in $CDCl_3$ at T = 310 K. (A) Experimental (the asterisk indicates an impurity) and (B) simulated spectrum.

P(2)–P(4) coupling. These phosphorus nuclei are in a *trans–trans* configuration and the value of $^3J(P–P)$ (156 Hz) used in the simulation falls in the range of coupling constants found in analogous platinum- and rhodium-containing clusters.[5,21–23,30,31] The match of experimental and simulated spectra supports the suggested spin–spin coupling model and suggests that the structure found in the solid state is retained in solution. The fact that the spectrum remains unchanged in the temperature range 220–310 K points to the stereochemical rigidity of the $Rh_2Pt_2(dppm)_2$ framework in **2**.

Careful treatment of the "lightly stabilized" $[Rh_6(CO)_{15}(NCMe)]$ cluster with a binuclear Pt(0) complex gave cluster **3**,

$$[Rh_6(CO)_{15}(NCMe)] + 2[Pt_2(CO)_3(dppm)_2] \xrightarrow[\text{THF, } -50\ ^\circ C \text{ Gentle heating to r.t.}]{N_2} [\{Rh_6(\mu_3\text{-}CO)_4(CO)_{10}\}(\mu_2\text{-}CO)_2\{Pt_4(dppm)_3\}] \quad (6)$$

3, 63%

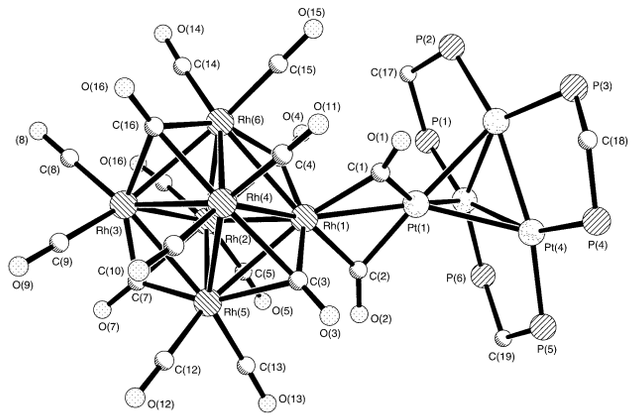

Fig. 5 Structure of $[\{Rh_6(\mu_3\text{-}CO)_4(CO)_{10}\}(\mu_2\text{-}CO)_2\{Pt_4(dppm)_3\}]$ (**3**).[6]

which contains coupled octahedral Rh_6 and tetrahedral Pt_4 frameworks. The solid-state structure of **3** has been earlier determined by an X-ray analysis.[6] The molecular structure of **3** is shown in Fig. 5, selected bond lengths and angles are given in Table 3.

The bonding of the two cluster units in **3** proved to be closely analogous to that in **2**, which implies the use of the dative (from Pt_4 to Rh_6) bond model to rationalize the electron count, which then gives 54 electrons for the Pt_4 and 86 electrons for the Rh_6 fragments. The structural motif of the ligand environment in the Pt_4 moiety is very similar to that found in a family of $MPt_3(dppm)_3$ clusters (M = Pt,[39] Re,[24,40–42] Ru)[31] which contain the Pt_3 basal triangle symmetrically bridged by three dppm ligands and an apical metal atom. The intercluster Pt–Rh bond length in **3** [2.6857(3) Å] is slightly shorter as compared with the corresponding Rh–Rh distance in **2** [2.7684(5) Å]. Bridging carbonyls span this bond in an asymmetric manner, both ligands being shifted to the Pt(1) atom. The structural parameters of the $Rh_6(CO)_{14}$ unit in **3** do not differ significantly from those found in **2**, including distortions in the coordination of the face-bridging C(3)O, C(4)O ligands. These observations also lend support to the assignment of the tetranuclear fragment in **3** as a two electron donor, similar to the bonding situation in **2**. The IR spectrum of **3** displays a pattern (2083m, 2050s, 2020m, 1772m br) typical for $[Rh_6(CO)_{16}]$-substituted derivatives[30,32,33] and a band (1977m br) corresponding to μ_2-bridging COs that is in complete agreement with the structure shown in Fig. 5. The ^{31}P spectrum of **3** exhibits one phosphorus resonance at −4.8 ppm with the satellite subspectrum typical for a symmetrical (C_{3v}) $Pt_3(dppm)_3$ moiety; see, for example, ref. 22 and 31, and references therein. This suggests that oscillation of the dppm ligands about the positions found in the solid-state structure results in the onset of three-fold symmetry on the basal $Pt_3(dppm)_3$, the metal to ligand connectivities remaining unchanged, as has been found for other similar clusters.[22,31]

Acknowledgements

Financial support from the Nordic Council of Ministers is gratefully acknowledged. We are also grateful to Professor D. H. Farrar (University of Toronto) for his support of the solid-state NMR experiments.

References

1 S. M. Waterman, N. T. Lucas and M. G. Humphrey, *Adv. Organomet. Chem.*, 2000, **46**, 47.
2 M. C. Comstock and J. R. Shapley, *Coord. Chem. Rev.*, 1995, **143**, 501.
3 P. Braunstein and J. Rose, in *Comprehensive Organometallic Chemistry*, ed. E. W. Abel, F. G. A. Stone and G. Wilkinson, Pergamon, Oxford, 2nd edn., 1994, vol. 10, ch. 7.

4 P. Braunstein and J. Rose, in *Catalysis by Di- and Polynuclear Metal Cluster Complexes*, ed. R. D. Adams and F. A. Cotton, Wiley-VCH, New York, 1998, p. 443.
5 F. M. Dolgushin, E. V. Grachova, B. T. Heaton, J. A. Iggo, I. O. Koshevoy, I. S. Podkorytov, D. J. Smawfield, S. P. Tunik, R. Whyman and A. I. Yanovskii, *J. Chem. Soc., Dalton Trans.*, 1999, 1609.
6 I. O. Koshevoy, S. P. Tunik, S. Jaaskelainen, M. Haukka and T. A. Pakkanen, *J. Chem. Soc., Dalton Trans.*, 2001, 2965.
7 M. C. Grossel, J. R. Batson, R. P. Moulding and K. R. Seddon, *J. Organomet. Chem.*, 1986, **304**, 391.
8 S. Schreiner and T. N. Gallaher, *Organometallics*, 1993, **12**, 4201.
9 L. Garlaschelli, P. Chini and S. Martinengo, *Gazz. Chim. Ital.*, 1982, **112**, 285.
10 S. Martinengo and P. Chini, *Gazz. Chim. Ital.*, 1972, **102**, 344.
11 S. Martinengo, P. Chini and G. Giordano, *J. Organomet. Chem.*, 1971, **27**, 389.
12 S. P. Tunik, A. V. Vlasov and V. V. Krivykh, *Inorg. Synth.*, 1997, **31**, 239.
13 Z. Otwinowski and W. Minor, *Methods Enzymol.*, 1997, **276**, 307.
14 P. T. Beurskens, G. Beurskens, R. de Gelder, S. Garcia-Granda, R. O. Gould, R. Israel and J. M. M. Smits, The DIRDIF-99 Program System. Technical Report of the Crystallography Laboratory, University of Nijmegan, The Netherlands, 1999.
15 L. J. Farrugia, *J. Appl. Crystallogr.*, 1999, **32**, 837.
16 A. Altomare, M. C. Burla, M. Camalli, G. L. Cascarano, C. Giacovazzo, A. Guagliardi, A. G. Moliterni, G. Polidori and R. G. Spagna, *Appl. Crystallogr.*, 1999, **32**, 115.
17 G. M. Sheldrick, SHELXTL, v. 5.1, Program for Crystal structure Determination, Siemens Analytical X-ray Instruments Inc., Madison, WI, USA, 1998.
18 G. M. Sheldrick, SHELXL97, Program for Crystal Structure Refinement, Siemens Analytical X-ray Instruments Inc., Madison, WI, USA, 1997.
19 P. Braunstein, J. Dehand and J. F. Nennig, *J. Organomet. Chem.*, 1975, **92**, 117.
20 J. P. Barbier, P. Braunstein, J. Fischer and L. Ricard, *Inorg. Chim. Acta*, 1978, **31**, L361.
21 B. T. Sterenberg, H. A. Jenkins and R. J. Puddephatt, *Organometallics*, 1999, **18**, 219.
22 B. T. Sterenberg, G. J. Spivak, G. P. A. Yap and R. J. Puddephatt, *Organometallics*, 1998, **17**, 2433.
23 G. J. Spivak, G. P. A. Yap and R. J. Puddephatt, *Polyhedron*, 1997, **16**, 3861.
24 J. L. Xiao, E. Kristof, J. J. Vittal and R. J. Puddephatt, *J. Organomet. Chem.*, 1995, **490**, 1.
25 S. Bhaduri, K. R. Sharma, W. Clegg, G. M. Sheldrick and D. Stalke, *J. Chem. Soc., Dalton Trans.*, 1984, 2851.
26 R. D. Adams, G. Chen, W. G. Wu and J. G. Yin, *Inorg. Chem.*, 1990, **29**, 4208.
27 S. P. Tunik, M. V. Osipov and A. B. Nikol'skii, *J. Organomet. Chem.*, 1992, **426**, 105.
28 S. P. Tunik, I. S. Podkorytov, B. T. Heaton, J. A. Iggo and J. Sampanthar, *J. Organomet. Chem.*, 1998, **550**, 221.
29 E. V. Grachova, B. T. Heaton, J. A. Iggo, I. S. Podkorytov, D. J. Smawfield, S. P. Tunik and R. Whyman, *J. Chem. Soc., Dalton Trans.*, 2001, 3303.
30 S. P. Tunik, A. V. Vlasov, K. V. Kogdov, G. L. Starova, A. B. Nikol'skii, O. S. Manole and Y. T. Struchkov, *J. Organomet. Chem.*, 1994, **479**, 59.
31 B. T. Sterenberg, M. C. Jennings and R. J. Puddephatt, *Organometallics*, 1999, **18**, 3737.
32 A. J. Poë and S. P. Tunik, *Inorg. Chim. Acta*, 1998, **268**, 189.
33 D. H. Farrar, E. V. Grachova, A. Lough, C. Patirana, A. J. Poë and S. P. Tunik, *J. Chem. Soc., Dalton Trans.*, 2001, 2015.
34 C. Babij, S. C. Browning, D. H. Farrar, I. O. Koshevoy, I. S. Podkorytov, A. J. Poë and S. P. Tunik, *J. Am. Chem. Soc.*, 2002, in press.
35 S. Rossi, K. Kallinen, J. Pursiainen, T. T. Pakkanen and T. A. Pakkanen, *J. Organomet. Chem.*, 1991, **419**, 219.
36 E. Corey, L. F. Dahl and W. Beck, *J. Am. Chem. Soc.*, 1963, **85**, 1202.
37 V. Albano and P. L. Bellon, *J. Organomet. Chem.*, 1969, **19**, 405.
38 J. Fisher, A. Mitchler, R. Weiss, J. Dehand and J. F. Nenning, *J. Organomet. Chem.*, 1975, **91**, C37.
39 G. Douglas, L. Manojlovic-Muir, K. W. Muir, M. C. Jennings, B. R. Lloyd, M. Rashidi, G. Schoettel and R. J. Puddephatt, *Organometallics*, 1991, **10**, 3927.
40 J. Xiao, J. J. Vittal, R. J. Puddephatt, L. Manojlovic-Muir and K. W. Muir, *J. Am. Chem. Soc.*, 1993, **115**, 7882.
41 J. Xiao, L. Hao, R. J. Puddephatt, L. Manojlovic-Muir, K. W. Muir and A. A. Torabi, *J. Chem. Soc., Chem. Commun.*, 1994, 2221.
42 L. J. Hao, J. L. Xiao, J. J. Vittal, R. J. Puddephatt, L. Manojlovic-Muir, K. W. Muir and A. A. Torabi, *Inorg. Chem.*, 1996, **35**, 658.